



# Uncooled long wavelength infrared photon detectors

J. Piotrowski<sup>a</sup>, A. Rogalski<sup>b,\*</sup>

<sup>a</sup> *Vigo System Ltd., 3 Świetlików Str., 01-397 Warsaw, Poland*

<sup>b</sup> *Institute of Applied Physics, Military University of Technology, 2 Kaliskiego Street, 49 00-908 Warsaw, Poland*

Available online 6 May 2004

## Abstract

Infrared (IR) photon detectors operating in the middle (3–5  $\mu\text{m}$ ) and long wavelength (8–14  $\mu\text{m}$ ) infrared spectral range require cryogenic cooling to achieve useful performance. The need for cooling is a major limitation of IR photon detectors what prevents more widespread use of IR technology. At present, uncooled thermal detector focal plane arrays are successfully used in staring thermal imagers. However, the performance of thermal detectors is modest, they suffer from slow response and they are not very useful in applications requiring multispectral detection. In the paper, a number of concepts to improve performance of photon detectors operating at room temperature are presented. Several types of detector materials are considered: HgCdTe, Sb-based III–V ternary alloys, and type-II InAs/GaInSb superlattice. Initial efforts were concentrated on photoconductors and photoelectromagnetic detectors. Recently, advanced heterojunction photovoltaic detectors have been developed. It is shown that uncooled HgCdTe photovoltaic detector can achieve detectivity of  $10^9 \text{ cm Hz}^{1/2} \text{ W}^{-1}$  at the 8–9  $\mu\text{m}$  range. Potentially the devices can be assembled in large focal plane arrays. This will enable obtaining of NEDT of less than 0.1 K for staring thermal imagers operating with  $f/l$  optics and  $30 \text{ s}^{-1}$  frame rate.

© 2004 Elsevier B.V. All rights reserved.

## 1. Introduction

Progress in infrared (IR) photon detector technology is mainly connected with semiconductor infrared detectors. The most important are photodetectors fabricated with narrow-gap semiconductors. To obtain high performance detectors, temperatures much lower than 300 K are required (typically 80–200 K). Cooling requirements significantly increase price and size of IR systems, therefore one of the main research goals is increase in working temperature of photodetectors. Affordable IR systems, such as IR imaging cam-

eras, require cost-effective detectors that operate without cooling or, at least, at temperatures compatible with long-life, low power and low cost coolers.

A number of concepts to improve performance of the near room temperature IR photodetectors have been proposed [1–3]. Apart from photoconductive detectors and photodiodes, three other types of IR photodetectors can operate at near room temperature; photoelectromagnetic (or PEM) detectors, magnetoconcentration detectors and Demer effect detectors [3]. While significant improvements have been obtained by suppression of Auger thermal generation in excluded photoconductors [4], extracted photodiodes [4–6], and magnetoconcentration effect detectors [7,8], these

\* Corresponding author. Tel./fax: +48-22-685-9109.

non-equilibrium devices require significant bias currents and exhibit excessive low frequency  $1/f$  noise that extends up to MHz range. The noise, which reduces the 800 Hz detectivity by 2–3 orders of magnitude compared to that measured at frequencies above the  $1/f$  knee ( $\sim 1$ – $10$  MHz), as well as the high current requirements is severe obstacle to their widespread applications.

Here we review progress in development of uncooled long wavelength infrared (LWIR) photon detectors. Different types of IR photodetectors especially photoconductors, photoelectromagnetic (PEM) detectors, Dember effect detectors and photodiodes with major emphasis on devices based on  $\text{Hg}_{1-x}\text{Cd}_x\text{Te}$  (HgCdTe) alloys are considered. Special attention is put on optimization of the devices for room temperature operation.

The review is mainly based on the authors experience in developing near room temperature HgCdTe detectors at the Institute of Applied Physics Military University of Technology and at Vigo System Ltd. An approach to reduce photodetector cooling requirements based of non-equilibrium mode of operation [4–6,9] and proposed by British workers is omitted in our considerations.

## 2. Fundamental performance limits of near room temperature photodetectors

The performance of infrared photodetectors is limited by statistical nature of generation and recombination of charge carriers in the semiconductor. Thermal processes dominate at near room temperature in materials used for middle and long wavelength devices. The detectivity of an optimized infrared photodetector is limited by thermal processes in the active region of the device. It can be expressed as [10]

$$D^* = 0.31 \frac{\lambda}{hc} k \left( \frac{\alpha}{G} \right)^{1/2}, \quad (1)$$

where  $1 \leq k \leq 2$ , and  $k$  is dependent on the contribution of recombination and backside reflection.

The ratio of the absorption coefficient to the thermal generation rate,  $\alpha/G$ , is the fundamental

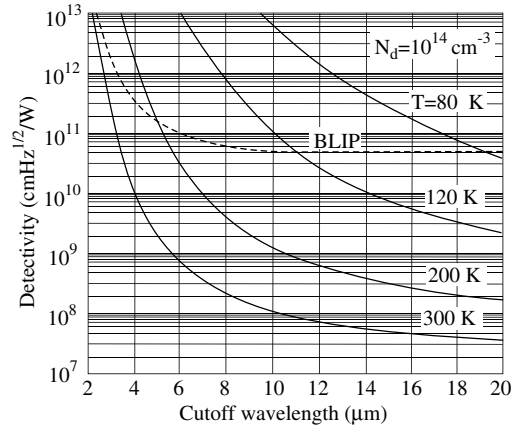


Fig. 1. Calculated performance of Auger generation-recombination limited HgCdTe photodetectors as a function of wavelength and temperature of operation. BLIP detectivity has been calculated for  $2\pi$  FOV, background temperature  $T_{\text{BLIP}} = 300$  K, and quantum efficiency  $\eta = 1$ .

figure of merit of any material intended for infrared photodetectors. This figure should be used to assess any potential material. Analysis shows, that the narrow gap semiconductors are more suitable for high temperature photodetectors in comparison to competing technologies such as extrinsic devices, Schottky barrier, and QWIP devices [11]. The main reason for high performance of intrinsic photodetectors is high density of states in the valence and conduction bands, which results in strong absorption of infrared radiation.

The Auger mechanism is likely to impose fundamental limitations to the LWIR HgCdTe detector performance. Fig. 1 shows the calculated detectivity of Auger generation-recombination limited HgCdTe photodetectors as a function of wavelength and temperature of operation. The calculations have been performed for doping level equal  $N_d = 10^{14} \text{ cm}^{-3}$ , as the lowest donor doping level, which at present is achievable in a controllable manner in practice. We can see that

- liquid nitrogen cooling potentially makes it possible to achieve BLIP performance in the wide 2–20  $\mu\text{m}$  range,
- 200 K cooling, which is achievable with Peltier coolers, would be sufficient for BLIP operation

in the middle and short wavelength IR regions (below 5 μm).

It is interesting to consider the performance requirements of near room temperature photodetectors for thermal cameras. Thermal resolution of infrared thermal systems is usually characterized by the noise equivalent temperature difference (NETD). It can be shown, that [12]

$$\text{NETD} = \frac{4F^2 \Delta f^{1/2}}{A_d^{1/2} t_{\text{op}}} \left[ \int_{\lambda_a}^{\lambda_b} \frac{dM}{dT} D^*(\lambda) d\lambda \right]^{-1}, \quad (2)$$

where  $F$  is the optics f-number,  $\Delta f$  is the frequency band,  $A_d$  is the detector area,  $t_{\text{op}}$  is the optics transmission,  $M$  is the spectral emittance of the blackbody described by the Plancks law.

As Eq. (2) shows, the thermal resolution improves with an increase in detector area. Increasing detector area results in reduced spatial resolution, however. Hence, a reasonable compromise between the requirement of high thermal and spatial resolution is necessary. Improvement of thermal resolution without spatial resolution worsening may be achieved by

- increase of detector area combined with corresponding increase of focal length and the objective aperture,
- improved detector performance,
- increase in number of detectors.

Increase of aperture is undesirable because it increases sizes, mass and price of an infrared system. It is more proper to use a detector with higher detectivity. Another possibility is the application of multi-elemental sensor, what reduces each element bandwidth proportionally to the number of elements for the same frame rate and other parameters.

Fig. 2 shows the dependence of detectivity on cutoff wavelength for a photon counter detector thermal imager with a resolution of 0.1 K. Detectivities of  $1.9 \times 10^8$ ,  $2.3 \times 10^8$ , and  $2 \times 10^9$  cm Hz<sup>1/2</sup>/W are necessary to obtain NETD = 0.1 K for 10, 9, and 5 μm cutoff wavelength photon counter detectors, respectively. The above estimations indicate, that the ultimate performance

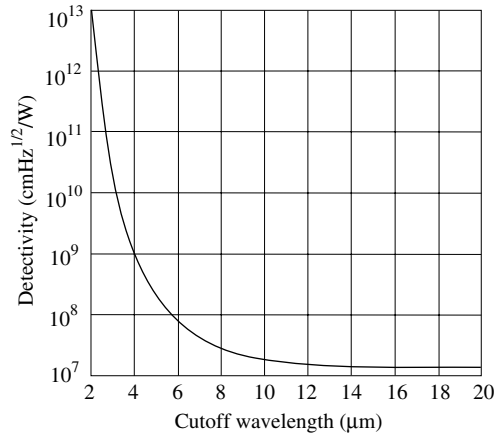


Fig. 2. Detectivity needed to obtain NETD = 0.1 K in a photon counter detector thermal imager as a function of cutoff wavelength.

of the uncooled photodetectors is not sufficient to achieve the required 0.1 K thermal resolution. The thermal resolution below 0.1 K is achieved for staring thermal imagers containing thermal detector focal plane arrays. Generally, the performance of thermal detectors are modest, they suffer from slow response, and they are not very useful in applications requiring multispectral detection.

### 3. Ways to improve detector's performance without cooling

There are some ways to improve the performance of the photodetectors without cooling. A moderate p-type doping of the absorber detector region is widely used for some suppression of the Auger mechanisms [1,2,4]. More efficient suppression can be obtained with non-equilibrium depletion of the semiconductor [4]. However, the non-equilibrium mode devices suffer from a high level of flicker noise that make them useless for most of practical applications that require detection of IR radiation in the low and moderate frequency range. An example is thermal imaging. Hence, non-equilibrium mode devices are omitted in our considerations.

A possible way to improve the performance of infrared detectors is to reduce the physical volume of the semiconductor, thus reducing the amount of thermal generation. This must be done without decrease in quantum efficiency, optical area, and field of view (FOV) of the detector.

### 3.1. Reduction of thickness

Thickness of the active region can be significantly reduced by enhanced absorption of radiation. This can be achieved by using multiple pass of radiation with a backside reflector. Even more efficient is the use of interference phenomena to set up a resonant cavity within the photodetector [1]. Various optical resonator structures have been proposed as shown in Fig. 3.

In the simplest method, interference occurs between the waves reflected at the rear, highly reflective surface and at the front surface of semiconductor. The thickness of the semiconductor is selected to set up the thermal standing waves in the structure with peaks at the front and nodes at the back surface. The quantum efficiency oscillates with thickness of the structure, with the peaks at a thickness corresponding to an odd multiple of  $\lambda/4n$ , where  $n$  is the refractive index of the semiconductor. The gain in quantum efficiency increases with  $n$ . Higher gain can be obtained in the structures shown in Fig. 3(b). There are some additional gains achieved in particular types of infrared detectors. Increased absorption makes

possible to improve collection efficiency in photodiodes since thickness can be made smaller than the diffusion length. Making use of interference effects, highly non-uniform absorption can be achieved even for long wavelength radiation with a low absorption coefficient, which is important for some devices such as photoelectromagnetic and Dember effect devices [1,3].

It should be noted that the interference effects strongly modify spectral response of the device. The gain due to the optical cavity can be achieved only in narrow spectral regions. This may be an important limitation for some applications that require wide spectral band sensitivity. In practice, infrared systems usually operate in a spectral band (e.g. atmospheric windows) and the use of resonant cavities may yield significant gains. Another limitation comes from the fact that efficient optical resonance occurs only for near-perpendicular incidence and is less effective for oblique incidence. This limits the use of the devices with fast optics.

### 3.2. Reduction of physical area of the detector

A possible way to improve the performance of infrared photodetector is an increase in apparent “optical” size of the detector in comparison with the actual physical size using a suitable concentrator which compresses impinging infrared radiation [1,2,13–15]. This must be achieved without reduction of the acceptance angle, or at least, with limited reduction to angles required for fast optics

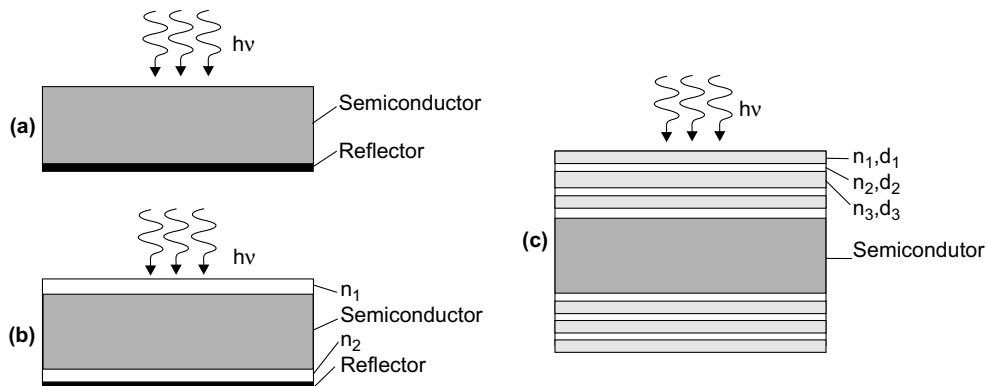


Fig. 3. Schematic structure of interference enhanced photodetectors: (a) the simplest structure, (b) structure immersed between two dielectric layers supplied with backside reflector, and (c) structure immersed between two photonic crystals.

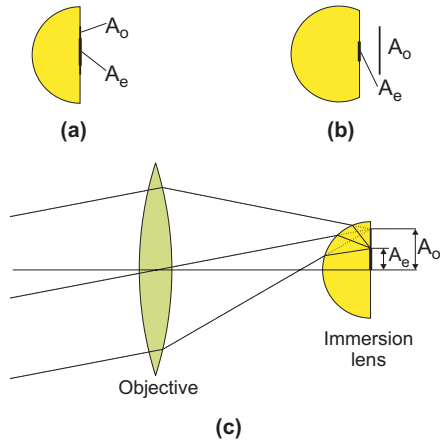


Fig. 4. Operation of hemispherical (a), hyperhemispherical (b) lens, and radiation running in objective/hemispherical lens optical system (c).

of infrared systems. Various types of suitable optical concentrators can be used, including optical cones and conical fibres. An efficient possible way to achieve an effective concentration of radiation is to immerse the photodetector to the hemispherical or hyperhemispherical lenses (see Fig. 4) [1,2]. The immersion lens plays the role of a field lens which increases the field of view of the optical system. The hyperhemisphere used as an aplanatic lens results in apparent increase in linear detector size by a factor of  $n^4$ .

Several factors must be taken into account in practical realization of the optically immersed detectors. Use of immersion technology has been limited due to problems with mechanical matching of detector and lens materials as well as severe transmission and reflection losses. Another limitation is due to the limited acceptance angle of the devices as a result of the total reflection at the lens-glass interface.

The problems of matching the detectors to immersion lenses have been solved by the use of monolithic technology developed at Vigo System [1]. The technology is based on epitaxy of HgCdZnTe on CdZnTe substrate. The HgCdZnTe serves as the sensitive element, while the immersion lens is formed directly in the transparent CdZnTe ( $n = 2.7$ ) or GaAs ( $n = 3.4$ ) substrates. For example, Fig. 5 shows schematically the

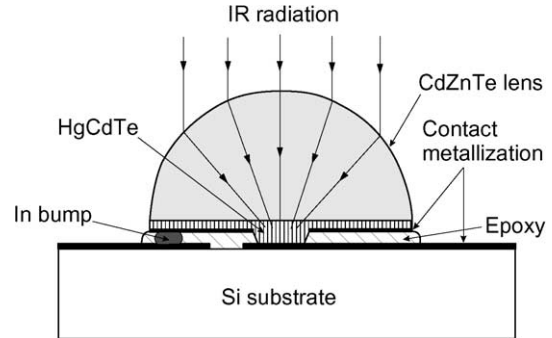


Fig. 5. Schematic cross-section of an experimental monolithic optically immersed Dember detector (after Vigo System data sheets, Warsaw, 1993).

structure of a monolithic optically immersed Dember detector.

Monolithic optical immersion results in significant improvement in detector parameters. The gain factors achieved with hyperhemispherical immersion are substantially higher compared to those for hemispherical immersion. The hyperhemispherical immersion may restrict the acceptance angle of the detector and require more severe manufacturing tolerances. These restrictions depend on the refraction coefficient of the lens. For CdZnTe, however, they are not so severe as for germanium lenses, and have no practical importance in many cases. For example, the numerical aperture of the main optical system is limited to about 1.4 by the CdZnTe immersion lens.

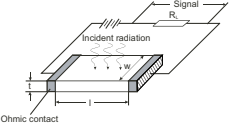
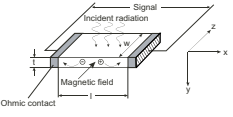
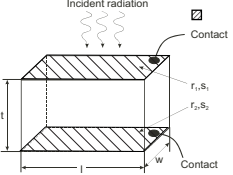
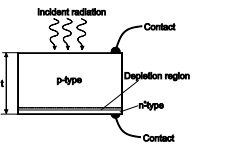
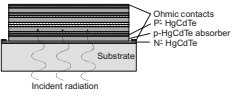
#### 4. Classical photon detectors for high temperature operation

The class of photon detectors is sub-divided into different types depending on how the electric or magnetic fields are developed (as shown in Table 1). Initial efforts to produce near room temperature LWIR photon detectors have concentrated mainly on optimization of photoconductors and PEM detectors [1–3].

##### 4.1. Photoconductors

Considerations carried out in Ref. [1] indicate that for optimally doped photoconductor at a high

Table 1  
HgCdTe uncooled photodetectors

Mode of operation	Schematic of detector	Advantages	Disadvantages	Performance (optically immersed, $\lambda = 10.6 \mu\text{m}$ )
Photoconductor		<ul style="list-style-type: none"> <li>• low cost technology</li> <li>• high responsivity</li> </ul>	<ul style="list-style-type: none"> <li>• bias required</li> </ul>	<p>at 300 K:</p> <ul style="list-style-type: none"> <li>• <math>D^*</math> up to <math>2 \times 10^8 \text{ cm Hz}^{1/2}/\text{W}</math></li> <li>• response time <math>\leq 1 \text{ ns}</math></li> </ul> <p>at 220 K:</p> <ul style="list-style-type: none"> <li>• <math>D^*</math> up to <math>3 \times 10^9 \text{ cm Hz}^{1/2}/\text{W}</math></li> <li>• response time <math>\leq 10 \text{ ns}</math></li> </ul>
PEM detector		<ul style="list-style-type: none"> <li>• no bias required</li> <li>• no flicker noise</li> <li>• very short response time</li> </ul>	<ul style="list-style-type: none"> <li>• bulky</li> <li>• low resistance</li> </ul>	<p>at 300 K:</p> <ul style="list-style-type: none"> <li>• <math>D^*</math> up to <math>1 \times 10^8 \text{ cm Hz}^{1/2}/\text{W}</math></li> <li>• response time <math>\leq 10 \text{ ns}</math></li> </ul>
Dember detector		<ul style="list-style-type: none"> <li>• no bias required</li> <li>• no flicker noise</li> </ul>	<ul style="list-style-type: none"> <li>• low resistance</li> <li>• require low resistance contacts</li> </ul>	<p>at 300 K:</p> <ul style="list-style-type: none"> <li>• <math>D^*</math> up to <math>1.5 \times 10^7 \text{ cm Hz}^{1/2}/\text{W}</math></li> <li>• response time <math>\leq 1 \text{ ns}</math></li> </ul>
Photodiode		<ul style="list-style-type: none"> <li>• fast response</li> <li>• no flicker noise</li> </ul>	<ul style="list-style-type: none"> <li>• very low dynamic resistance</li> <li>• low quantum efficiency</li> <li>• influence of series resistance</li> </ul>	<p>at 220 K (multielement array):</p> <ul style="list-style-type: none"> <li>• <math>D^*</math> up to <math>2 \times 10^8 \text{ cm Hz}^{1/2}/\text{W}</math></li> <li>• response time <math>\leq 3 \text{ ns}</math></li> </ul>
Stacked multi-heterojunction photodiode		<ul style="list-style-type: none"> <li>• high dynamic resistance</li> <li>• good quantum efficiency</li> <li>• no flicker noise</li> <li>• extremely fast response</li> <li>• can be use from DC to very high frequencies</li> </ul>	<ul style="list-style-type: none"> <li>• influence of series resistance</li> </ul>	<ul style="list-style-type: none"> <li>• generation-recombination limit of performance can be achieved in practice at any wavelength</li> <li>• practical implementation requires well established epitaxial technology</li> </ul>

bias, the detectivity is limited by generation-recombination noise and is equal to

$$D^* = 0.45 \frac{\lambda}{hc} y^{1/2}, \quad (3)$$

where

$$y = \frac{\alpha\tau(z + 1/z)}{n_i}. \quad (4)$$

In the above equations  $\lambda$  is the wavelength of radiation,  $h$  is the Planck's constant,  $c$  is the light velocity,  $z = p/n_i$ ,  $n_i$  is the intrinsic concentration,  $p$  is the hole concentration,  $\alpha$  is the absorption coefficient, and  $\tau$  is the carrier lifetime. At low bias when thermal noise prevails, the detectivity increases with bias voltage.

From Eq. (3) results advantage to fabricate near room temperature photoconductors from p-type materials, since absorption coefficient and recombination time achieve their maximum value at  $z \approx 2$ . A further increase in doping results in decrease of  $y$ , mainly due to the rapid decrease in the Auger recombination lifetime.

To achieve maximum performance, very good bias power dissipation is required, what is difficult to realize in practice. The highest measured detectivity of uncooled 10.6  $\mu\text{m}$  photoconductors at high frequency is about  $6 \times 10^7 \text{ cm Hz}^{1/2} \text{ W}^{-1}$ , this value is a factor of  $\sim 2.5$  below the theoretical limit. The commercially available devices have detectivities of about  $1 \times 10^7 \text{ cm Hz}^{1/2} \text{ W}^{-1}$  (see [www.vigo.com.pl](http://www.vigo.com.pl)). A moderate cooling, which can be conveniently done with one or several stage thermoelectrical coolers, can improve the performance. The improvement in performance is, however, accompanied by an increase in a response time. The peak wavelength of 10.6  $\mu\text{m}$  optimized device is shorter than 10.6  $\mu\text{m}$  for which the device was optimized. The shift increases with decreasing thickness, and in commercial devices with low bias power, the peak responsivity is at 6–7  $\mu\text{m}$ .

Typical structure of uncooled photoconductor is similar to cooled device. The optimum thickness of the active elements (a few microns) depends upon the temperature of operation and is smaller in uncooled devices. The sensitive elements are housed in various packages, the examples of which are shown in Fig. 6. The packages are usually



Fig. 6. Examples of uncooled and thermoelectrically cooled single element photodetectors manufactured by Vigo System, Warsaw.

designed to minimize parasitic impedances as the ambient temperature photoconductors are capable of high frequency operation with a typical bandwidth of  $\sim 200 \text{ MHz}$ , achieving  $\sim 1 \text{ GHz}$  in high-frequency optimized devices.

#### 4.2. PEM detectors

The PEM effect has been traditionally used for room temperature detectors in the middle- and far-infrared band. Cooling of the PEM detectors poses problems associated with the use of a magnet and results in little improvement in device performance. Advantages of the PEM detector are lack of bias and low resistance, enabling the use of fast electronics.

For a long time InSb has been the most common material for photoelectromagnetic detectors. Their properties have been reviewed by Kruse [16]. InSb with maximum performance at about 6.5  $\mu\text{m}$  exhibit no response in the 8–14  $\mu\text{m}$  atmospheric window and relatively modest performance in the 3–5  $\mu\text{m}$  window, however.  $\text{Hg}_{1-x}\text{Cd}_x\text{Te}$  (HgCdTe) and closely related  $\text{Hg}_{1-x}\text{Zn}_x\text{Te}$  (HgZnTe) and  $\text{Hg}_{1-x}\text{Mn}_x\text{Te}$  (HgMnTe) alloys made possible to optimize performance of PEM detectors at any specific wavelength [2,3].

The PEM effect is caused by diffusion of photogenerated carriers due to the photo-induced

carrier concentration gradient and by deflection of electron and hole trajectories in opposite directions by the magnetic field (see Table 1). If the sample ends are open-circuit in the  $x$ -direction, a space charge builds up giving rise to an electric field along the  $x$  axis (open-circuit voltage). If the sample ends are short-circuited in the  $x$ -direction, a current flows through the shorting circuit (short-circuit current).

Theoretical analysis indicates that the maximum voltage responsivities of PEM detectors can be reached in relatively strong magnetic fields ( $B \approx 1/\mu_c$ ). For materials such as  $\text{Hg}_{1-x}\text{Cd}_x\text{Te}$ , where  $\mu_c/\mu_h \gg 1$ , the resistance of the detector reaches its maximum value at the point  $p/n_i \approx (\mu_c/\mu_h)^{1/2}$  and the highest value for voltage responsivity is reached for lightly doped p-type material. The acceptor concentration in narrow gap semiconductors is adjusted to a level of about  $(2-3) \times 10^{17} \text{ cm}^{-3}$  [1–3]. At room temperature, the ambipolar diffusion length in narrow gap semiconductors is small (several  $\mu\text{m}$ ) while the absorption of radiation is relatively weak ( $1/\alpha \approx 10 \mu\text{m}$ ). In such cases the radiation is almost uniformly absorbed within the diffusion length. Thus, a low recombination velocity at the front surface and a high recombination velocity at the back surface are necessary for a good PEM detector response [3]. In such devices, the polarity of signal reverses with a change of illumination direction from the low to the high recombination velocity surface, while the responsivity remains almost unchanged.

The preparation of PEM detectors is similar to that of photoconductive ones, with the exception of the back surface preparation which in PEM devices is subjected to a special mechanochemical treatment to achieve a high recombination velocity. This procedure is not mandatory when using graded gap structures. The wafers are thinned to final thickness of about  $5 \mu\text{m}$  and cut into bars sized  $\sim 1 \times 2 \text{ mm}^2$ . Electrical contacts are usually made by gold electroplating to the ends of the bars, to which gold wires are then attached.

Fig. 7 shows schematically the housings of PEM detectors, which are based on standard TO-5 or, for larger elements, TO-8 transistor cans. The

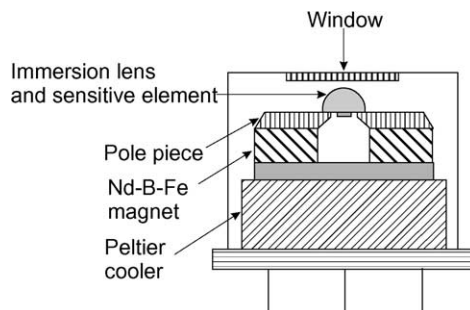


Fig. 7. Schematic of the housing of a thermoelectrically cooled, optically immersed PEM detector (after Vigo System data sheets, Warsaw, 1993).

active elements are mounted in a housing which incorporates a miniature two-element permanent magnet and pole pieces. Magnetic fields approaching 2 T are achievable with the use of modern rare-earth magnetic materials for the permanent magnet and cobalt steel for the pole pieces.

The best uncooled  $\text{HgCdTe}$   $10.6 \mu\text{m}$  PEM detectors exhibited measured voltage responsivity of about  $0.1 \text{ V/W}$  (width of 1 mm) and detectivities of about  $1 \times 10^7 \text{ cm Hz}^{1/2} \text{ W}^{-1}$  which is by a factor of  $\sim 3$  below the predicted ultimate value.

Both the theoretical and the measured performance of PEM detectors are inferior to that of photoconductive detectors. PEM detectors have, however, additional advantages, which make them useful in many applications. In contrast to photoconductors, they do not require electrical biasing. The frequency characteristics of a PEM detector is flat over a wide frequency range, starting from constant current. This is due to lack of low frequency noise and a very short response time. The response time, which is determined by effective recombination time is less than the bulk recombination time. As short response times, as 50 ps, are easily achievable in devices optimized for high frequency operation, with little expense in responsivity. The resistances of PEM detectors do not decrease with increasing size what makes possible to achieve potential performance in large size devices. With the resistance typically close to  $50 \Omega$ , the devices are conveniently coupled directly to wideband amplifiers.



Magnetoconcentration effect detector is a relatively new device [3,7,8] that can be related to non-equilibrium mode devices. The geometry of the device is the same as that of conventional PEM detectors, but the device is biased with an electric field perpendicular to the magnetic field and oriented in such a way that the Lorentz force, acting on the current carriers, directs them to the surface of high surface recombination velocity. In effect, the concentration of electrons and holes in the bulk of the material is diminished and thus the regions become depleted. This leads to suppression of thermal generation and recombination processes and in consequence in reduction of thermally generated noise. However, the high bias current requirements and significant  $1/f$  noise in this type of detector have been severe obstacles to their widespread applications.

#### 4.3. Dember effect detectors

Dember effect detectors are a type of photovoltaic devices, based on bulk photodiffusion voltage in a simple structure with only one type of semiconductor doping. The use of the Dember effect for high temperature long-wavelength detectors has been suggested by Piotrowski et al. [1,17]. When radiation is incident on the surface of a semiconductor, a potential difference is usually developed in the direction of the radiation (see Table 1). This is known as photodiffusion or the Dember effect. Two conditions are required for generation of the photovoltage: the distribution of photogenerated carriers should be non-uniform and the diffusion coefficients of electrons and holes must be different. The gradient usually results from non-uniform optical generation and from different surface recombination velocities at the front and back surfaces of the device. The Dember effect electrical field restrains the electrons with higher mobility, while holes are accelerated, thus making both fluxes equal. The best performance is achievable for a device thickness of the order of a diffusion length, low recombination velocity at the front and high at the back surface.

As in the case of the PEM detector, the best performance is achieved in p-type material. The

Dember detector is not biased and the noise voltage is determined by the Johnson–Nyquist thermal noise. Also the response time of Dember detectors is determined by processes analogous to those used for PEM detectors.

The calculated detectivity of 200–300 K Dember detectors is higher compared to that of photoconductors operated under the same conditions. However, very low resistances, low voltage responsivities and noise voltages well below the noise level of the best amplifiers pose serious problems in achieving the potential performance. For example, uncooled 10.6  $\mu\text{m}$  devices with size  $50 \times 50 \mu\text{m}^2$  will have a resistance of  $\approx 0.15 \Omega$  and noise voltage of  $\approx 50 \text{ pV/Hz}^{1/2}$ . This explains why the conventional Dember detectors cannot compete with other types of photodetectors [3].

There are some potential ways to overcome this difficulty. One is the connection of small area Dember detectors in series. For example, to obtain reasonable resistance ( $\approx 50 \Omega$ ) in a  $1 \text{ mm}^2$  total area sensitive element of an uncooled 10.6  $\mu\text{m}$  detector, it is necessary to divide its area into 400  $50 \times 50 \mu\text{m}^2$  elements, connected in series with low resistance interconnections, which is feasible with modern fabrication.

The other possibility is to use optical immersion. Detectivities as high as  $\approx 1.7 \times 10^9$  and  $1.5 \times 10^{10} \text{ cm Hz}^{1/2}/\text{W}$  are expected at 300 and 200 K in optimized optically immersed 10.6  $\mu\text{m}$  devices [17].

Due to ambipolar diffusion of excess carriers the response time of a Dember detector is shorter than the bulk recombination time and can be very short for devices with thickness much less than the diffusion length [1]. The response time of optimized devices is about 1 ns, shortening with p-type doping, with some expense in performance. The high frequency optimized Dember detectors should be prepared from heavily doped material and the thickness should be kept low. For example, for detectors with  $N_a = 5 \times 10^{17} \text{ cm}^{-3}$  and  $t = 2 \mu\text{m}$ ,  $\tau$  is  $\approx 50 \text{ ps}$ . Another possible limitation of response time, the RC constant, is not important due to a low resistivity and low capacity of the Dember detector.

Manufacturing of Dember detectors from Hg-based narrow gap semiconductors requires

well-established technology of devices from bulk crystals or epilayers. Fig. 5 shows a schematic of a monolithic optically immersed uncooled Dember effect detector manufactured by VIGO. The sensitive element has been prepared from an  $\text{Hg}_{1-x}\text{Cd}_x\text{Te}$  epitaxial layer grown with the hyperhemispherical lens formed directly in the transparent  $\text{CdZnTe}$  substrate. The surface of the sensitive element was subjected to a mechanochemical treatment to produce a high recombination velocity and covered with reflecting gold. The “electrical” size of the sensitive element is  $7 \times 7 \mu\text{m}^2$  while, due to the hyperhemispherical immersion, the apparent optical size is increased to  $\approx 50 \times 50 \mu\text{m}^2$ . The measured voltage responsivity was  $\approx 100 \text{ V/W}$ , which is about one order of magnitude below the calculated value for an optimized device.

Large active area devices ( $>100 \mu\text{m}$  square) are produced by connections of small element in series. Although they are less sensitive, they can successfully compete with photoconductors in applications requiring very low frequency or/and very high frequency operation.

Recently, the volume Dember effect is combined with photovoltaic effect at heterojunctions resulting in better response.

#### 4.4. Photodiodes

As early as in 1975, Koehler and Chiang [18] reported  $n^+p$   $10.6 \mu\text{m}$  photodiodes operated at 170 K. Shanley et al. [19] showed a capability of achieving bandwidths of 475–725 MHz, quantum efficiency of 78%, an  $R_0A$  product of  $0.006 \Omega\text{cm}^2$  and fairly good heterodyne sensitivity of  $1.3 \times 10^{19} \text{ W/Hz}$  at a temperature of 145 K. Extension of operational temperature to 185–200 K was suggested with a proper adjustment of bandgap and doping level. Gordon [13] discussed possible operation of a  $9.5 \mu\text{m}$  photodiode array using optical immersion with microlenses at temperatures 150–245 K. The practical 128-element array based on the loophole technology with silicon microlenses has been reported by Jones et al. [14]. At 192 K and wavelength of  $9 \mu\text{m}$  detectivities of  $4 \times 10^9 \text{ cm Hz}^{1/2}/\text{W}$  have been achieved.

The voltage responsivity of a homojunction photodiode with photoelectrical gain of unity is

$$R_v = \frac{\eta\lambda}{hc} R_d, \quad (5)$$

where  $R_d = dI/dV$  is the diode differential resistance. Assuming negligible effect of background radiation, the zero bias noise is determined by the Johnson–Nyquist noise and detectivity of zero biased photodiode is

$$D^* = \frac{\eta\lambda}{2hc} \left( \frac{R_0A}{kT} \right)^{1/2}. \quad (6)$$

As Eq. (6) shows, for the best performance, the value  $\eta(R_0A)^{1/2}$  should be optimized for given wavelength and temperature. Simple consideration indicate that due to high mobility of electrons, the  $n^+p$  structure photodiodes offer the best performance (better  $R_0A$  product and quantum efficiency).

The photovoltaic device of conventional design suffers from

- poor quantum efficiency, and
- low differential resistance.

Only charge carriers that are photogenerated at distance shorter than the diffusion length from junction can be collected. The absorption depth of long wavelength IR radiation ( $\lambda > 5 \mu\text{m}$ ) is longer than the diffusion length. Therefore, only a limited fraction of the photogenerated charge contributes to the quantum efficiency. Consider an example of an uncooled  $10.6 \mu\text{m}$  photodiode. Calculations show that the ambipolar diffusion length is less than  $2 \mu\text{m}$  while the absorption depth is  $\approx 13 \mu\text{m}$ . This reduces the quantum efficiency to  $\approx 15\%$  for single pass of radiation through the detector.

The resistance of the  $p-n$  junction is very low due to a high thermal generation. In materials with a high electron to hole mobility ration, the resistance is additionally reduced by ambipolar effects [8]. As a result, the preamplifier noise and noise of parasitic resistances may exceed the thermal generation-recombination noise. As a result, the performance of conventional devices is very poor, so they are not usable for practical applications.

**5. Uncooled HgCdTe devices with improved performance**

The above described two methods—enhanced absorption and reduction of physical area—have been applied in various types of uncooled infrared photodetectors developed and manufactured at Vigo System. The devices were initially based on variable gap HgCdTe heterostructures grown by isothermal vapour growth epitaxy (ISOVPE) in a proprietary reusable growth system, which also enables *in situ* doping with foreign impurities [20]. The first uncooled LWIR devices were photoconductors, photoelectromagnetic and Dember effect detectors described in Section 4. Later, they have been replaced with photovoltaic detectors which do not require electric or magnetic bias.

Fig. 8 shows the spectral detectivities of ambient temperature optically immersed photoconductive and PEM HgCdTe detectors. The highest measured detectivity of 10.6 μm room temperature photoconductor at high frequency (0.1–100 MHz) is about  $6 \times 10^7 \text{ cm Hz}^{1/2} \text{ W}^{-1}$ , which is a factor of  $\approx 2.5$  below the theoretical limit. The  $1/f$  noise is especially stringent in uncooled devices, which require a high biasing for the best performance. Applications of these detectors include fast pyrometers, spectroscopy, and gas analyzers. Two-stage Peltier cooled photoconductors, with re-

sponse time of 0.01–3 μs in dependence on spectral range, are applied in fast pyrometers, simple thermal imagers, conventional and Fourier spectroscopy, gas analysis, and laser warning devices.

Ambient temperature PEM detectors with response time <0.1 ns are optimized for detection of 10.6 μm CO<sub>2</sub> laser radiation. These detectors do not exhibit flicker noise and are suitable for detection in both continuous wave (CW) and high frequency modulated radiation.

The present generation of uncooled LWIR devices is based on photovoltaic devices [21–26]. The problems of poor quantum efficiency and large series resistance have been solved through adoption of sophisticated heterojunction architectures of photovoltaic devices in combination with the methods of reduction of physical size of active element.

An efficient improvement was development of multiple heterojunction photovoltaic devices to increase the voltage responsivity of the devices. Practical realization of the multi-heterojunction device consisted of a structure based on backside illuminated n<sup>+</sup>-p-P photodiodes (symbol “+” denotes strong doping, capital letter—wider gap) has been presented in several papers [21–25]. The individual detector elements were prepared by a combination of conventional dry etching, angled ion milling, and angled thermal evaporation for

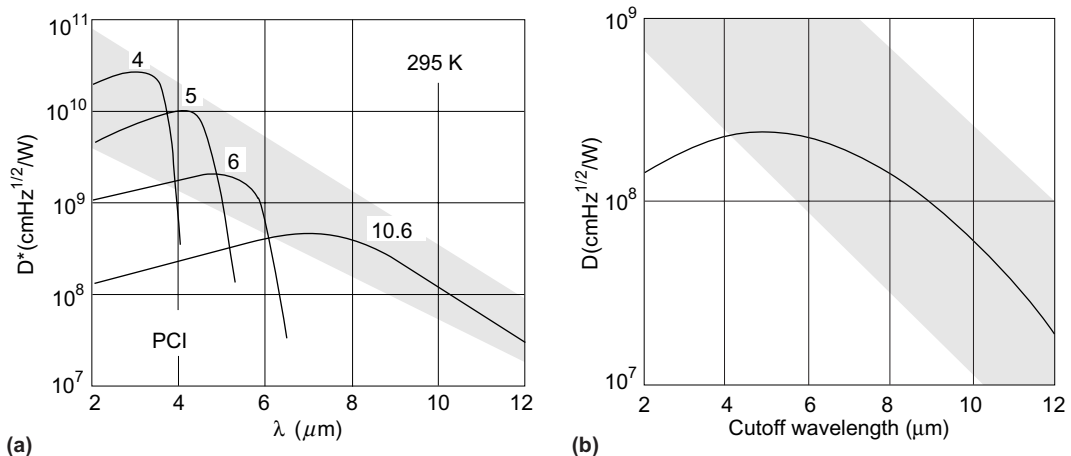


Fig. 8. Spectral detectivities of optically immersed HgCdTe photodetectors: (a) photoconductive detectors and (b) PEM detector. Numbers indicate the wavelengths in micrometers for which the device is optimized.

contact metal deposition (see Fig. 9). p-type active layer with thickness of approximately 10  $\mu\text{m}$  and doping levels about  $10^{16} \text{ cm}^{-3}$  were grown on CdZnTe substrates using ISOVPE (LPE) and in situ As (Sb) doping. Recently, MOCVD growth on GaAs has been applied. The epitaxial layers exhibited near uniform composition in the uppermost 2/3 of the total thickness, while a significant grading occurred in the lower portion of the layer with the bandgap increasing toward the substrate. The delineation trenches in the epilayer were wet chemical etched using Br/ethylene glycol or Br/HBr solutions to a depth of 2/3 of the thickness of epilayer. The etch was followed by shallow ion beam milling using a Kaufman-type ion gun. The sample was placed at  $\approx 45^\circ$  to the direction of the  $\text{Ar}^+$  beam so that only one wall of the trench was exposed to the beam. The ion beam milling results in n-type conversion and the formation of  $n^+p$  junctions on the uppermost surface and on one side of the trench walls. Due to the grading of the epilayer composition and doping with depth, the final structure approximates a  $n^+p$  photodiode. Cr/Au metallization was required to provide external contact to the device and to short-circuited  $N^+P^+$  junction formed at the base of trench, effectively connecting side-by-side diodes in series. As a final step, the devices were passivated by thermal evaporation of 200 nm of CdZnTe followed by 300 nm of ZnS. For an epilayer  $\approx 8 \mu\text{m}$  thick, the minimum practical multi-junction period using existing wet etching technology is  $\approx 10 \mu\text{m}$ .

Fig. 10 shows the room temperature spectral response of HgCdTe multi-heterojunction devices monolithically immersed to the CdZnTe lens. The

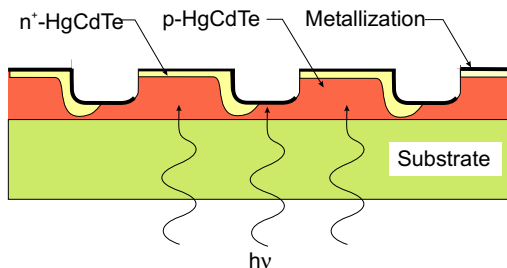


Fig. 9. Backside illuminated multiple heterojunction device.

devices were based on multiple junctions with a period of 15–30  $\mu\text{m}$ . Generally, these room temperature devices have responsivities that are comparable to, or better than, photoelectromagnetic devices operating under the same conditions. Peltier cooled devices exhibit performance that is comparable to photoconductors operating at the same wavelength and temperatures. However, in contrast to photoconductors, multi-heterojunction detectors can be used at both low and very high frequencies. Heterodyne experiments indicate that the response time of LWIR devices at a wavelength of 10.6  $\mu\text{m}$  is only of about 1 ns.

The critical issue of multiple HgCdTe photodiodes is parasitic impedances, frequent occurrence of reverse polarity photovoltages at the contacts between P and  $N^+$  regions located in the wide bandgap material, which should be short-circuited by metallization. Another problem may arise from requirement of a very small size of individual element (for LW room temperature devices the optimum length of an individual element is below 5  $\mu\text{m}$ ) which makes difficult to achieve a high ratio of the active to the dead areas. Moreover, such devices suffer from the non-uniform response across the active area. These problems have been mostly overcome and the devices are commercially available at present. The devices

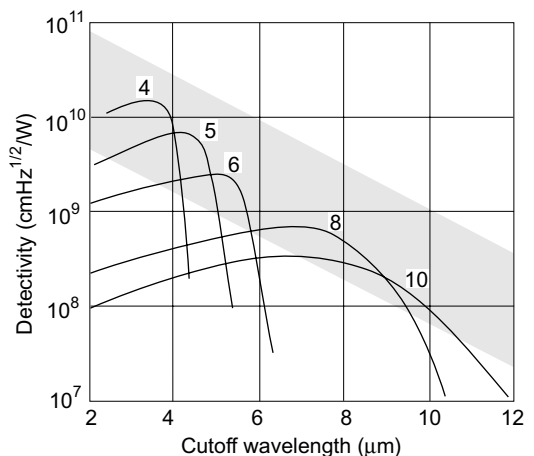


Fig. 10. Measured detectivity of multi-heterojunction uncooled HgCdTe detectors. Optical immersion has been used to improve the performance.

are manufactured as single devices optimized for any wavelength within the 2–16  $\mu\text{m}$  range, with active area sizes from a few micrometers to a few millimetres. Linear arrays up to 120 elements and small 2D arrays are manufactured as custom devices.

Optical immersion has been used almost exclusively for single element devices. The use of a single immersion lens to a large array is problematic in view of optical aberrations and the large lens size. The problem can be solved by implementation of a small size 2D array monolithically integrated with microlenses. The small size of active element ( $\approx 7 \times 7 \mu\text{m}$ ) is beneficial for good collection of photogenerated charge carriers especially in LWIR devices. The individual elements can be accessed individually or connected in series.

The devices are especially promising as uncooled 7.8–9.5  $\mu\text{m}$  detectors that can be used for thermal imagers. Initial results are encouraging, indicating the potential for achieving  $\approx 10^9 \text{ cm Hz}^{1/2}/\text{W}$  at  $\lambda \approx 9 \mu\text{m}$ . This would enable thermal resolution better than 0.1 K for staring thermal imagers operating with  $f/1$  optics. Moreover, the devices exhibit very fast response with a time constant of  $\approx 1 \text{ ns}$ . This is due to the short time required for photogenerated carriers in small size active region to reach heavily doped contacts and a short RC time constant as well.

In multiple heterojunction devices described previously (see Fig. 9), the junction's planes are perpendicular to the surface. More promising are the stacked multijunction photodiodes monolithically connected in series, what is shown in Fig. 11. They are capable of achieving both good quantum efficiency and a large differential resistance. Each

cell is composed of p-type doped narrow gap absorber and heavily doped  $\text{N}^+$  and  $\text{P}^+$  heterojunction contacts. The incoming radiation is absorbed only in absorber regions, while the heterojunction contacts collect the photogenerated charge carriers. Detectivity achieves a maximum for 15 cells. For practical reasons, the number of cells could be reduced to  $\approx 10$ , with detectivity more than doubled in comparison to a single cell device. The device can be supplied with backside reflectors for double pass of infrared radiation, optical resonant cavities and optical concentrators, such as immersion lenses. For 10.6  $\mu\text{m}$  device containing 5 cells and operated at room temperature, detectivity over to  $10^9 \text{ cm Hz}^{1/2}/\text{W}$  can be achieved [26]. Practical implementation of the device would require well establish low temperature epitaxial growth (MBE or MOCVD).

## 6. Alternative uncooled long wavelength infrared photon detectors

HgCdTe has been the most important intrinsic semiconductor material for both cooled and uncooled LWIR photodetector applications. But at the same time, HgCdTe is one of the most difficult materials to use for infrared detectors because of the problem caused by lattice, surface, and interface instabilities. These problems originate from weak bonding characteristics of II–VI semiconductors and from high Hg vapour pressure. Weak bonding reduces strength of material, resulting in a bad mechanical property and creating difficulties in material processing. Moreover high Hg vapour pressure makes the composition control over a

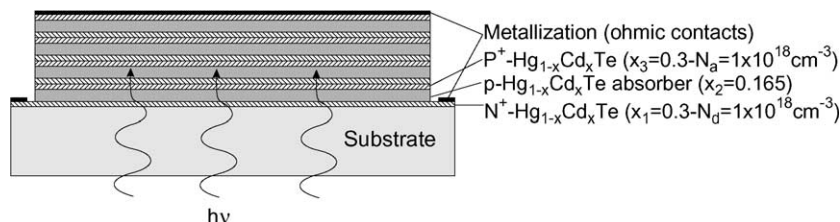


Fig. 11. Schematic cross-section of the 4-cells stacked multiple detector. The backside illuminated device is supplied with reflector for double pass of infrared radiation.

large area difficult, causing serious problems for the focal plane arrays applications. This intensified the search for alternative infrared material systems.

As alternative to the current market dominant HgCdTe, a number of III–V semiconductor systems such as  $\text{InAs}_{1-x}\text{Sb}_x$  (InAsSb) [27–29],  $\text{InSb}_{1-x}\text{Bi}_x$  (InSbBi) [30,31],  $\text{In}_{1-x}\text{Tl}_x\text{Sb}$  (InTlSb) [31], and InAs–GaSb type-II superlattices have been proposed [32].

Earlier data suggest that  $\text{InAs}_{1-x}\text{Sb}_x$  can exhibit a cutoff wavelength up to  $12.5\ \mu\text{m}$  at 300 K (the minimum of energy gap appears at composition  $x = 0.65$ ) [27]. However, some recent experimental results demonstrated that the cutoff wavelength of epitaxial layers can be longer than  $12.5\ \mu\text{m}$ , thus covering the entire 8– $14\ \mu\text{m}$  at near room temperature. This may be due to structural ordering.

InAsSb photoconductive detectors are based on p-InAsSb/p-InSb heterostructures. A room temperature photoresponse up to  $\approx 14\ \mu\text{m}$  has been obtained at 300 K [28]. From the voltage dependent responsivity measurement, an effective lifetime of about 0.14 ns has been obtained. The estimated detectivity at  $\lambda = 10.6\ \mu\text{m}$  is limited by Johnson noise at the level of about  $3 \times 10^7\ \text{cm Hz}^{1/2}/\text{W}$  at 300 K.

Photovoltaic devices consist of a double heterojunction of  $\text{p}^+-\text{InSb}/\pi-\text{InAs}_{1-x}\text{Sb}_x/\text{n}^+-\text{InSb}$  on (001)GaAs (see Fig. 12(a)). In spite of the large lattice mismatch between the InAsSb and GaAs, InAsSb detectors have exhibited good characteristics and showed their feasibility for the near room temperature LWIR photodetectors. The photodiode optimized for  $\lambda = 10.6\ \mu\text{m}$  was characterized by the voltage responsivity-area product of  $3 \times 10^{-5}\ \text{V cm}^2/\text{W}$  and detectivity of  $\approx 1.5 \times 10^8\ \text{cm Hz}^{1/2}\ \text{W}^{-1}$ . Preliminary experiments on the biased mode operation of the InAsSb heterojunction photodiodes shown that the voltage responsivity at near room temperature has been increased by a factor of  $\approx 3$  at 0.4 V reverse bias (see Fig. 12(b)). Further increase in responsivity can be achieved through lower doping level.

Since  $\text{InAs}_{0.35}\text{Sb}_{0.65}$ -based detector is not sufficient for efficient infrared detection in the 8– $12\ \mu\text{m}$  range, InTlSb was proposed as a potential infrared material at LWIR region [33]. TlSb is predicted as a semimetal. By alloying TlSb with InSb, the band gap of InTlSb could be varied from  $-1.5$  to 0.26 eV. Assuming a linear dependence of the band gap on alloy composition,  $\text{In}_{1-x}\text{Tl}_x\text{Sb}$  can then be expected to reach a band gap of 0.1 eV at  $x = 0.08$  while exhibiting a similar lattice constant as InSb

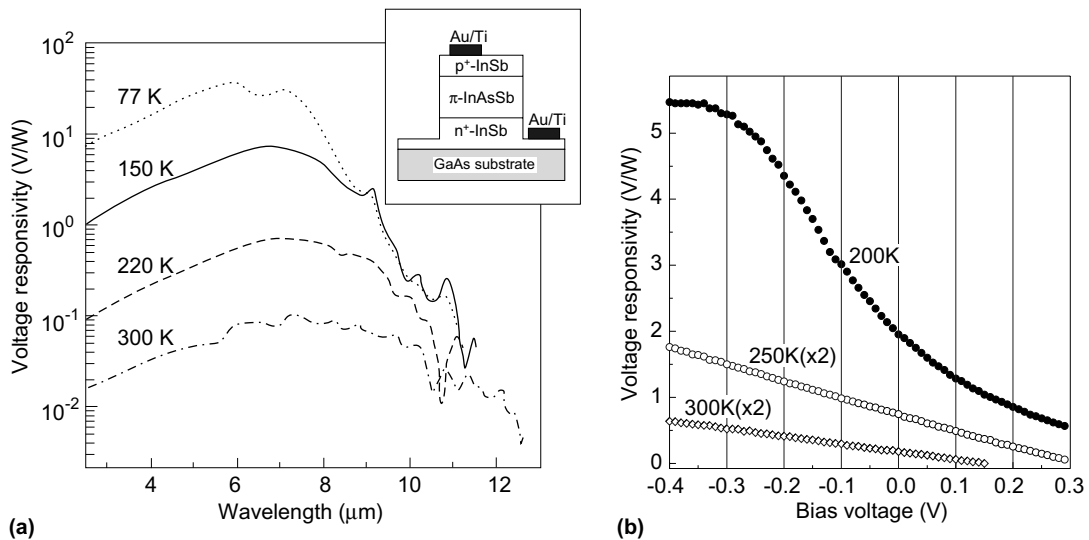


Fig. 12.  $\text{p}^+-\text{InSb}/\pi-\text{InAs}_{0.15}\text{Sb}_{0.85}/\text{n}^+-\text{InSb}$  heterojunction photodiode: spectral voltage responsivity (schematic of a photodiode structure in the insert) (a) and bias dependent voltage responsivity (b) (after Ref. [28]).

since the radius of Tl atom is very similar to In. At this gap, InTlSb and HgCdTe have very similar band structure. This implies that InTlSb has comparable optical and electrical properties to HgCdTe. In structural aspect, InTlSb is expected to be more robust due to stronger bonding. Room temperature operation of InTlSb photodetectors has been demonstrated with a cutoff wavelength of about 11  $\mu\text{m}$  [31].

As another alternative to the HgCdTe material system,  $\text{InSb}_{1-x}\text{Bi}_x$  has been considered because the incorporation of Bi into InSb produces a rapid reduction in the band gap of 36 meV/%Bi. Thus, only a few percent of Bi is required for reduction of the band gap energy.

The growth of InSbBi epitaxial layer is difficult due to the large solid phase miscibility gap between InSb and InBi. Recently, the successful growth of InSbBi epitaxial layer on InSb and GaAs (100) substrates with substantial amount of Bi ( $\sim 5\%$ ) has been demonstrated using low-pressure MOCVD [30,31]. The responsivity of  $\text{InSb}_{0.95}\text{Bi}_{0.05}$  photoconductor at 10.6  $\mu\text{m}$  is  $1.9 \times 10^{-3}$  V/W at room temperature and the corresponding Johnson-noise limited detectivity is  $1.2 \times 10^6$   $\text{cm Hz}^{1/2}/\text{W}$ . The effective carrier lifetime estimated from bias voltage-dependent responsivity is about 0.7 ns at 300 K.

Type-II superlattices have been proposed as another alternative for infrared photodetectors in the LWIR range. In comparison to HgCdTe, the higher effective mass of electrons and holes and the slower Auger recombination rate lead to lower dark current and higher operating temperature in type-II superlattices. Unlike type-I superlattices, one can modify the energy of the conduction and valence minibands of a type-II superlattice with a high degree of freedom. The InAs–GaInSb type-II superlattices have shown promising results in the LWIR range at low temperatures [34]. However, recently published results have shown that this material system is very promising for uncooled LWIR detectors [32]. Perhaps the most important problem is still the growth of type-II detectors since the overall performance of the device greatly depends on superlattice quality.

InAs–GaSb superlattices were grown by MBE on semi-insulating (001)GaAs substrates. Photo-

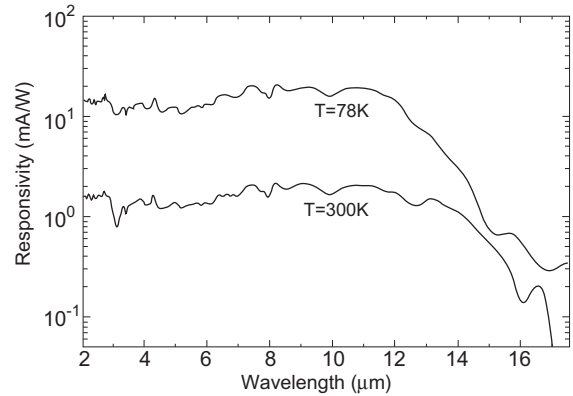


Fig. 13. The responsivity spectra of the device at 78 and 300 K with an in-plane electrical field of 5 V/cm (after Ref. [32]).

conductive detectors fabricated from the superlattices showed 80% cutoff at about 12  $\mu\text{m}$ . The responsivity of the device (see Fig. 13) is about 2 mA/W with a 1 V bias (electrical field 5 V/cm) and the maximum measured detectivity of the device is  $1.3 \times 10^8$   $\text{cm Hz}^{1/2}/\text{W}$  (without any immersion lens and antireflector coating) at 11  $\mu\text{m}$  at room temperature. The detector shows very weak temperature sensitivity. The carrier lifetime,  $\tau = 26$  ns, is an order of magnitude longer than the carrier lifetime in HgCdTe with similar bandgap and carrier concentration. This evidences suppression of Auger recombination in this material system.

## 7. Conclusions

Photodetectors are based on photogeneration of electrons and holes in a semiconductor material, followed by subsequent collection of the created charge. They have important advantages compared to the thermal detectors. Since no thermal processes are involved in a detection process, photodetectors exhibit very fast response. No thermal insulation is necessary. In contrast to thermal detectors, the performance of photodetectors exponentially decreases with increasing cutoff wavelength and temperature of operation. As a result, the uncooled LWIR devices are typically characterized by poor performance.

Uncooled LWIR photodetectors are less developed compared to the competition thermal

detectors, however. Their availability is limited to single element and small arrays. The main problem is their low resistance that prevents use of well developed CCD and CMOS readout circuits. This can be solved with development of integrated microoptics, multiple heterojunctions, and Auger suppressed devices.

Currently, the only commercially available fast room temperature detectors in the LWIR range are HgCdTe photodetectors. New materials, InAsSb, InTlSb, InSbBi, and type-II superlattices have demonstrated the capability to provide uncooled performance equivalent to thermal detectors with cutoff frequencies orders of magnitude higher. Being grown on the GaAs substrates, these III–V material systems are promising for the future integration with Si technology. However, hitherto, no practical devices based on this technology are available.

At present, uncooled thermal detectors are clearly the winner in the race for uncooled thermal imaging. At the same time, further improvement in thermal and spatial resolution of thermal imagers based on FPAs with thermal detectors remains a substantial challenge. For thermal detectors it will require clever design to include an IR absorber in a very low mass pixel structure. Future development may involve devices based on new principles of operation.

Photon detectors offer also an advantage for multispectral operation. Poor performance, availability of suitable image processors and high cost, are the main issues of uncooled LWIR devices for imaging applications. They are devices of choice for high frequency applications, however.

## References

- [1] J. Piotrowski, W. Galus, M. Grudzień, Near room-temperature IR photodetectors, *Infrared Phys.* 31 (1991) 1–48.
- [2] J. Piotrowski, Hg<sub>1-x</sub>Cd<sub>x</sub>Te detectors, in: A. Rogalski (Ed.), *Infrared Photon Detectors*, SPIE Optical Engineering Press, Bellingham, 1995, pp. 391–493.
- [3] J. Piotrowski, A. Rogalski, Photoelectromagnetic, magnetoconcentration and Dember infrared detectors, in: P. Capper (Ed.), *Narrow-Gap II–VI Compounds and Electromagnetic Applications*, Chapman & Hall, London, 1997, pp. 506–525.
- [4] C.T. Elliott, N.T. Gordon, Infrared detectors, in: C. Hilsom (Ed.), *Handbook on Semiconductors*, 4, North-Holland, Amsterdam, 1993, pp. 841–936.
- [5] C.T. Elliott, Non-equilibrium mode of operation of narrow-gap semiconductor devices, *Semicond. Sci. Technol.* 5 (1990) S30–S37.
- [6] T. Elliott, New infrared and other applications of narrow gap semiconductors, *Proc. SPIE* 3436 (1998) 763–775.
- [7] Z. Djuric, J. Piotrowski, Infrared photodetector with electromagnetic carrier depletion, *Opt. Eng.* 31 (1992) 1955–1960.
- [8] J. Piotrowski, W. Gawron, Z. Djuric, New generation of near-room-temperature photodetectors, *Opt. Eng.* 33 (1994) 1413–1421.
- [9] C.T. Elliott, Photoconductive and non-equilibrium devices in HgCdTe and related alloys, in: P. Capper, C.T. Elliott (Eds.), *Infrared Detectors and Emitters: Materials and Devices*, Kluwer Academic Publishers, Boston, 2001, pp. 279–312.
- [10] J. Piotrowski, W. Gawron, Ultimate performance of infrared photodetectors and figure of merit of detector material, *Infrared Physics and Technology* 38 (1997) 63–68.
- [11] A. Rogalski, Quantum well photoconductors in infrared detectors technology, *J. Appl. Phys.* 93 (2003) 4355–4391.
- [12] A. Rogalski, *Infrared Detectors*, Gordon and Breach, Amsterdam, 2000.
- [13] N.T. Gordon, Design of Hg<sub>1-x</sub>Cd<sub>x</sub>Te infrared detector arrays using optical immersion with microlenses to achieve a higher operation temperature, *Semicond. Sci. Technol.* 8 (1991) C106–C109.
- [14] C.L. Jones, B.E. Matthews, D.R. Purdy, N.E. Metcalfe, Fabrication and assessment of optically immersed CdHgTe detector arrays, *Semicond. Sci. Technol.* 6 (1991) 110–113.
- [15] M.E. Motamedi, W.E. Tennant, H.O. Sankur, R. Melendes, N.S. Gluck, S. Park, J.M. Arias, J. Bajaj, J.G. Pasko, W.V. McLevige, M. Zandian, R.L. Hall, P.D. Richardson, Micro-optic integration with focal plane arrays, *Opt. Eng.* 36 (1997) 1374–1381.
- [16] P.W. Kruse, Indium antimonide photoconductive and photoelectromagnetic detectors, in: R.K. Willardson, A.C. Beer (Eds.), *Semiconductors and Semimetals*, 5, Academic Press, 1970, pp. 15–83.
- [17] Z. Djuric, J. Piotrowski, Dember IR photodetectors, *Solid-State Electron.* 34 (1991) 265–269.
- [18] T. Koehler, A.M. Chiang, Advanced HgCdTe for infrared applications, *Proc. SPIE* 62 (1975) 26–36.
- [19] J.F. Shanley, C.T. Flanagan, M.B. Reine, Elevated temperature n<sup>+</sup>-p Hg<sub>0.8</sub>Cd<sub>0.2</sub>Te photodiodes for moderate bandwidth infrared heterodyne applications, *Proc. SPIE* 227 (1980) 117–122.
- [20] J. Piotrowski, Z. Nowak, M. Grudzień, W. Galus, K. Adamiec, Z. Djuric, V. Jovic, Z. Djinovic, High capability, quasi-closed growth system for isothermal vapour phase epitaxy of (Hg,Cd)Te, *Thin Solid Films* 161 (1988) 157–169.



- [21] J. Piotrowski, W. Gawron, Extension of longwavelength IR photovoltaic detector operation to near room-temperatures, *Infrared Phys. Technol.* 36 (1995) 1045–1051.
- [22] C. Musca, J. Antoszewski, J. Dell, L. Faraone, J. Piotrowski, Z. Nowak, Multi-heterojunction large area HgCdTe long wavelength infrared photovoltaic detector for operation at near room temperature, *J. Electron. Mater.* 27 (1998) 740–746.
- [23] J. Piotrowski, Z. Nowak, J. Antoszewski, C. Musca, J. Dell, L. Faraone, A novel multi-heterojunction HgCdTe long-wavelength infrared photovoltaic detector for operation under reduced cooling conditions, *Semicond. Sci. Technol.* 13 (1998) 1209–1214.
- [24] W. Gawron, A. Rogalski, HgCdTe buried multi-junction photodiodes fabricated by the liquid phase epitaxy, *Infrared Phys. Technol.* 43 (2002) 157–163.
- [25] J. Piotrowski, M. Grudzień, Z. Nowak, Z. Orman, J. Pawluczyk, M. Romanis, W. Gawron, Uncooled photovoltaic  $\text{Hg}_{1-x}\text{Cd}_x\text{Te}$  LWIR detectors, *Proc. SPIE* 4130 (2000) 175–184.
- [26] J. Piotrowski, P. Brzozowski, K. Józwiowski, Stacked multijunction photodetectors of long wavelength radiation, *J. Electron. Mater.* 32 (2003) 672–676.
- [27] A. Rogalski,  $\text{InAs}_{1-x}\text{Sb}_x$  infrared detectors, *Prog. Quantum Electron.* 13 (1989) 191–231.
- [28] J.D. Kim, M. Razeghi, Investigation of InAsSb infrared photodetectors for near-room temperature operation, *Opto-Electron. Rev.* 6 (1998) 217–230.
- [29] E. Michel, M. Razeghi, Recent advances in Sb-based materials for uncooled infrared photodetectors, *Opto-Electron. Rev.* 6 (1998) 11–23.
- [30] J.L. Lee, M. Razeghi, Exploration of InSbBi for uncooled long-wavelength infrared photodetectors, *Opto-Electron. Rev.* 6 (1998) 25–36.
- [31] J.J. Lee, M. Razeghi, Novel Sb-based materials for uncooled infrared photodetector applications, *J. Cryst. Growth* 221 (2000) 444–449.
- [32] H. Mohseni, J. Wojkowski, M. Razeghi, G. Brown, W. Mitchel, Uncooled atmospheric window InAs-GaSb type-II infrared detectors grown on GaAs substrates for the 8–12  $\mu\text{m}$ , *IEEE J. Quantum Electron.* 35 (1999) 1041–1044.
- [33] A.B. Chen, M. Van Schilfgaarde, A. Sher, Comparison of  $\text{In}_{1-x}\text{Ti}_x\text{Sb}$  and  $\text{Hg}_{1-x}\text{Cd}_x\text{Te}$  as long wavelength infrared materials, *J. Electron. Mater.* 22 (1993) 843–846.
- [34] L. Bürkle, F. Fuchs, InAs/(GaIn)Sb superlattices: a promising material system for infrared detection, in: M. Henini, M. Razeghi (Eds.), *Handbook of Infrared Detection Technologies*, Elsevier, Oxford, 2002, pp. 159–189.